iScience

CellPress
OPEN ACCESS

Article

# Single-cell RNA sequencing of murine ankle joints over time reveals distinct transcriptional changes following *Borrelia burgdorferi* infection

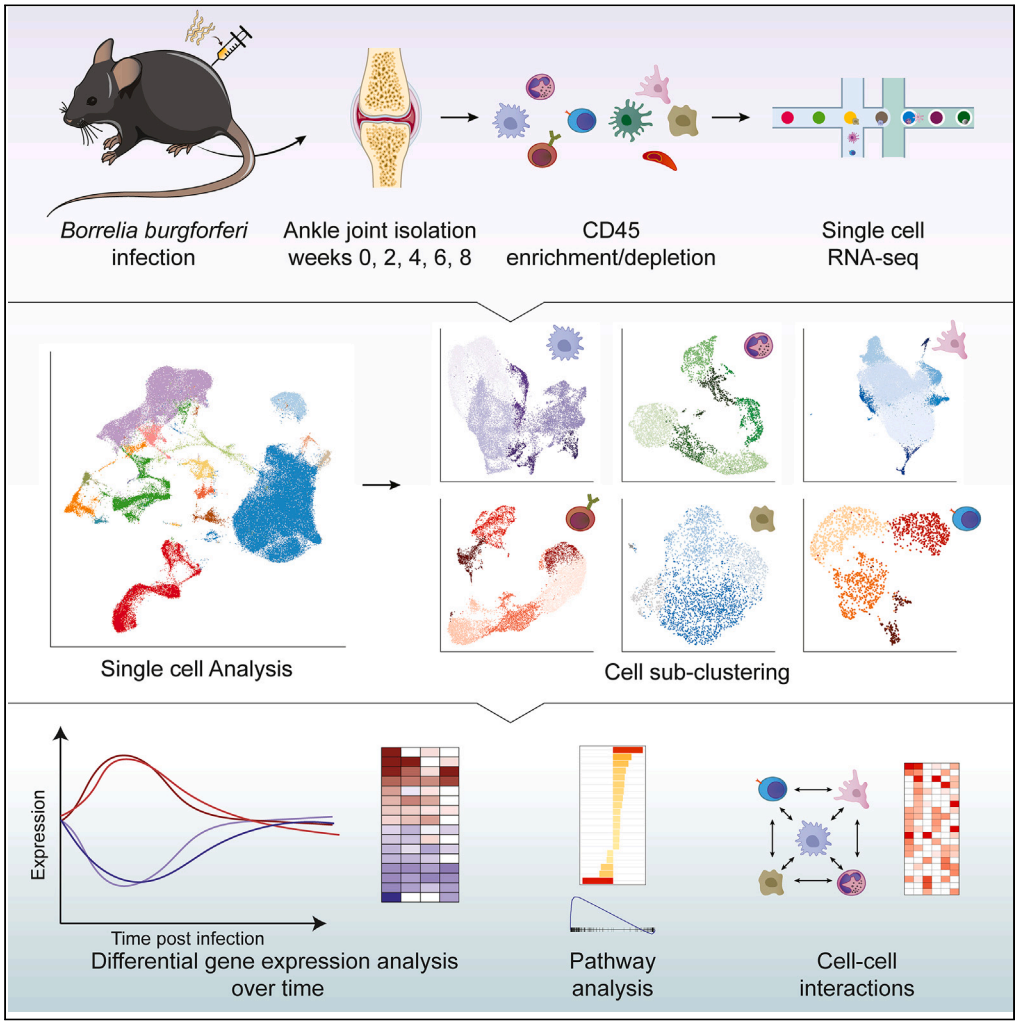


Jennifer D. Helble, Michael J. Walsh, Julie E. McCarthy, ..., Benjamin Y. Arnold, Alexandra-Chloe Villani, Linden T. Hu

linden.hu@tufts.edu

## Highlights

Single cell transcriptomic time course of *Borrelia burgdorferi* infection in mice

Several major cell types exhibit interferon gene signatures following infection

Inflammatory signature in cells peaks early and return to baseline

Cell-cell interactions suggest macrophages communicate with multiple cell types

Helble et al., iScience 26, 108217
November 17, 2023 
https://doi.org/10.1016/j.isci.2023.108217

iScience

CellPress
OPEN ACCESS

Article

# Single-cell RNA sequencing of murine ankle joints over time reveals distinct transcriptional changes following *Borrelia burgdorferi* infection

Jennifer D. Helble,[1] Michael J. Walsh,[2,3] Julie E. McCarthy,[1] Neal P. Smith,[4] Alice J. Tirard,[4] Benjamin Y. Arnold,[4] Alexandra-Chloe Villani,[4] and Linden T. Hu[1,5,*]

## SUMMARY

**Lyme disease is caused by the bacterial pathogen *Borrelia burgdorferi*, which can be readily modeled in laboratory mice. In order to understand the cellular and transcriptional changes that occur during *B. burgdorferi* infection, we conducted single-cell RNA sequencing (scRNA-seq) of ankle joints of infected C57BL/6 mice over time. We found that macrophages/monocytes, T cells, synoviocytes and fibroblasts all showed significant differences in gene expression of both inflammatory and non-inflammatory genes that peaked early and returned to baseline before the typical resolution of arthritis. Predictions of cellular interactions showed that macrophages appear to communicate extensively between different clusters of macrophages as well as with fibroblasts and synoviocytes. Our data give unique insights into the interactions between *B. burgdorferi* and the murine immune system over time and allow for a better understanding of mechanisms by which the dysregulation of the immune response may lead to prolonged symptoms in some patients.**

## INTRODUCTION

*Borrelia burgdorferi* is a causative agent of Lyme disease, which is the most common vector-borne disease in the United States.[1] While cases of Lyme disease are most geographically concentrated in the Northeast, mid-Atlantic, and Midwest states, there are still estimates of almost 500,000 cases annually in the United States alone.[2,3] Lyme disease occurs when *B. burgdorferi* is transmitted by an *Ixodes scapularis* tick vector into the skin of a human during feeding. At the bite site, *B. burgdorferi* causes a characteristic erythema migrans rash; however, the bacterium can quickly disseminate into other tissues in the body. Although antibiotics are effective against infection, untreated infection in humans can lead to various inflammatory diseases of peripheral tissues, including arthritis, carditis and meningitis.[4,5]

Lyme arthritis, characterized by inflammation and swelling of the joints (most commonly, the knees in humans and the ankle joints in mice), is one of the later disease manifestations to arise and is a common symptom of Lyme disease in the U.S. if the infection is not treated early.[4] Various inflammatory mediators have been shown to be present in synovial fluid and/or joint tissue, including the cytokine interferon gamma (IFNγ). IFNγ has pleiotropic functions but has been shown to change the cellular immune composition of the joint toward a more inflammatory phenotype during *B. burgdorferi* infection.[6,7]

Inflammation of the joints due to *B. burgdorferi* infection can be readily modeled in several strains of inbred laboratory mice, including C3H and C57BL/6 mice. Although C57BL/6 mice develop less severe joint inflammation and Lyme arthritis compared to C3H,[8] C57BL/6 mice are an attractive model to use to understand the transcriptional and cellular changes that occur during *B. burgdorferi* over time as there are substantially more knockout mice in this background compared to other strains that can be used for future studies.[4] Additionally, it is unclear whether the responses of mouse strains that develop either severe or mild arthritis more closely mimic human Lyme arthritis. For example, through forward genetic studies, it has been demonstrated that C3H mice are driven to more severe arthritis by a defect in a glycogen storage gene that has not been reported to be a risk factor for human disease.[9] Of note, even without antibiotic therapy, most humans with Lyme arthritis will spontaneously resolve their symptoms over time,[5,10] similar to what is observed in both C3H and C57BL/6 mice, although the time to resolution in humans is longer than it is for mice. In mice, the resolution of arthritis occurs despite the continued presence of the organism and likely reflects both a decrease in the numbers of organisms in the joint over time and an evolution of the immune response as it adapts to long-term infection with an organism that does not present a significant threat to the animal.

[1]Department of Molecular Biology and Microbiology, Tufts University School of Medicine, Boston, MA 02111, USA
[2]Division of Gastroenterology, Massachusetts General Hospital, Boston, MA 02114, USA
[3]Department of Cancer Immunology and Virology, Dana Farber Cancer Institute, Boston, MA 02215, USA
[4]Department of Medicine, Massachusetts General Hospital, Boston, MA 02114, USA
[5]Lead contact
*Correspondence: linden.hu@tufts.edu
https://doi.org/10.1016/j.isci.2023.108217

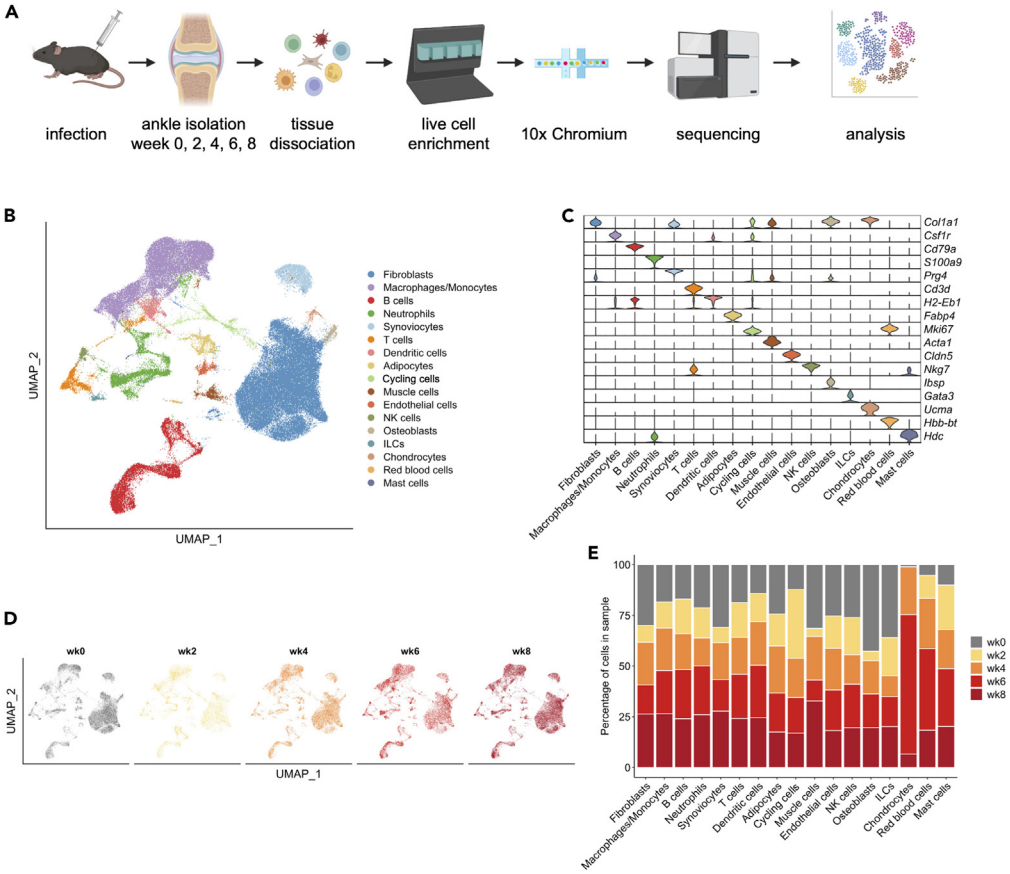


**Figure 1. Single-cell RNA sequencing of the mouse ankle joint reveals 17 distinct cell types**

(A) Schematic representation of the experimental set up. Ankle joints were harvested from mice at week 0 (uninfected), 2, 4, 6, and 8 post-inoculation and were enzymatically digested to obtain a single cell suspension. Live cells were magnetically sorted and single cell libraries were prepared and sequenced using the Chromium 10x platform, followed by downstream data analysis.

(B and C) 17 distinct cell clusters were identified using the *Seurat* R package and (B) visualized using the Uniform Manifold Approximation and Projection (UMAP).

(C) Violin plot of cluster defining genes.

(D) UMAPs showing the distribution of cells between time points and (E) bar plot showing relative contributions of each cell type over time.

See also Figures S1, S3, and S4, and Tables S1, S4, and S5.

In this study, we sought to assess transcriptional changes that occur in response to *B. burgdorferi* infection in the ankle joints of C57BL/6 mice. To this end, we performed single-cell RNA sequencing (scRNA-seq) to transcriptionally profile cells, identify population heterogeneity, and analyze how cellular environments change over time. Sequencing of immune and non-immune cells in the mouse ankle joint was performed over five distinct time points, starting with uninfected animals and progressing to eight weeks post-infection in two-week increments. From this dataset, we identified 17 different major cell populations in the ankle joint, including macrophages, B cells, neutrophils, T cells, fibroblasts, and synoviocytes. Of these major cell populations, we found that most transcriptional changes occurred between uninfected and the week two post-infection time point. Our findings provide a valuable resource for studying the host response to *B. burgdorferi* infection and could afford insight into the cellular implications of human Lyme arthritis.

## RESULTS

### Single-cell RNA sequencing of murine ankle joints following *Borrelia burgdorferi* infection reveals 17 distinct cell populations

To determine the cellular composition of the murine ankle joint following *B. burgdorferi* infection, we performed scRNA-seq of ankle joints of uninfected and infected C57BL/6 mice at zero (uninfected), two, four, six and eight weeks post-infection (Figure 1A). Single-cell suspensions obtained from uninfected and infected mice were filtered for live cells and further separated into $CD45^+$ and $CD45^-$ pools through subsequent magnetic enrichment. $CD45^+$ and $CD45^-$ cells were processed separately but analyzed together. Low quality cells were removed based on gene counts/cell and mitochondrial reads (high-quality cells that made it through these filters are visualized in Figures S1A–S1C), leaving a total of 119,086 high-quality cells originating from 38,682 $CD45^+$ and 80,404 $CD45^-$ sorted samples, which were integrated together.

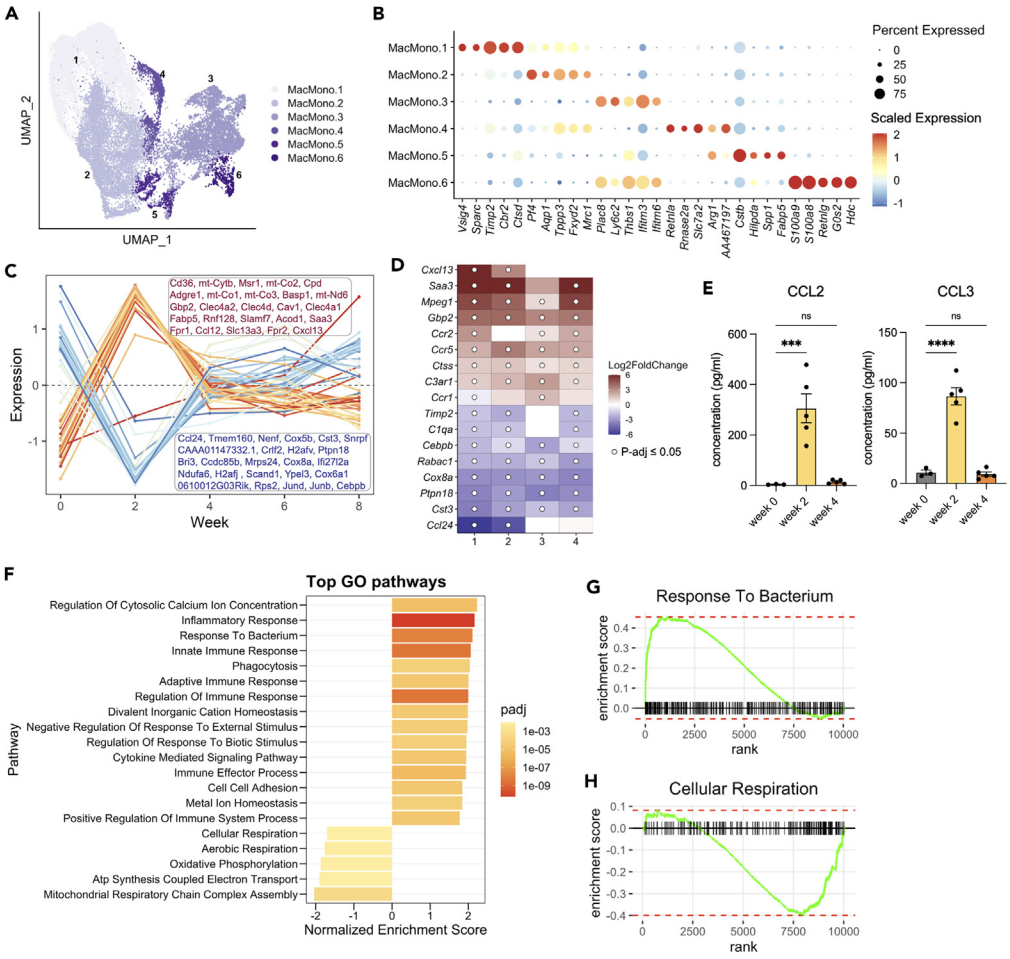


**Figure 2. Characterization of macrophages and monocytes in the ankle joint reveals broad transcriptional changes between uninfected and week two post-infection**

(A) Macrophages/monocytes identified previously were re-clustered to exclude doublets and visualized using a UMAP revealing 6 distinct sub-clusters.

(B) Cluster defining genes were identified using FindAllMarkers.

(C) Pseudobulk analysis of MacMono.1 cluster, showing the top 50 most significant genes changing over time. The 25 genes with a positive (red, top box) or negative (blue, bottom box) log2 fold change between week 0 and week 2 are shown.

(D) Heatmap of a subset of genes identified during pseudobulk analysis of MacMono.1 shown across all macrophage/monocyte clusters. Genes that are significantly different between uninfected and week 2 have a white dot in the center.

(E) Re-analyzed cytokine array of CCL2 and CCL3 production in ankle joints of mice over time from Helble et al.[12] Data were analyzed using ordinary one-way analysis of variance (ANOVA) with Dunnett's multiple comparisons test and are representative of at least 3 mice per group and are represented as the mean ± SEM; ***$p < 0.001$, and ****$p < 0.0001$.

(F) GSEA of GO biological processes was performed using pseudobulk analysis of week 0 vs. week 2 from the MacMono.1 sub-cluster.

(G and H) Select GSEA enrichment plots from GO pathways identified in F) with a G) positive and H) negative enrichment score.

See also Figure S2 and Tables S2 and S3.

Unbiased clustering of cells revealed 17 distinct cell populations (Figure 1B) that were identified based on expression of cluster-defining genes (Figures 1C and S1D). Samples contributed fairly evenly to cell coverage (Figure 1D), with 29,373 cells ($CD45^-$ and $CD45^+$) from uninfected mice; 13,589; 23,804; 21,850; and 30,470 cells from two, four, six, and eight weeks, respectively. Cell frequencies across the weeks sampled were consistent, except for chondrocytes (Figure 1E).

## Macrophage and monocytic populations undergo rapid transcriptional changes in response to *Borrelia* infection

Based on total cells recovered from the single cell transcriptional profiling of the ankle joint (Figure 1B), macrophages and monocytes were the predominant immune cell population present. To understand their contribution to the immune response to *B. burgdorferi* infection, we re-clustered these cells to remove doublets (Figures S2A and S2B) and then performed a final re-clustering to reveal six macrophage/monocyte clusters (Figure 2A). The resulting macrophage/monocyte sub-clusters each had a unique set of cluster-defining genes (Figure 2B;

Table S1) and were represented across all weeks (Figures S2C and S2D). To further contextualize these sub-populations, we performed Gene Set Enrichment Analysis (GSEA) comparing gene expression of each sub-cluster (all weeks combined) to all other sub-clusters using a previously identified M1/M2 gene signature in mouse bone marrow derived macrophages.[11] While we found that MacMono.3 and MacMono.6 were enriched for M1 genes and MacMono.4 was enriched for M2 genes, the other three sub-clusters exhibited a mixed gene signature (Figure S2E).

To evaluate transcriptional changes over time, we performed pseudobulk differential expression analysis for the four largest macrophage/monocyte clusters (MacMono.1 through MacMono.4) (Table S2). We decided to focus on the macrophage/monocyte cluster, MacMono.1, as it was both the largest cluster and did not fall into the classical M1/M2 categorization. We found that for the MacMono.1 sub-cluster, there were large transcriptional differences that occurred between uninfected and week 2 post-infection (Figure 2C). Interestingly, many of these genes returned to baseline at week four post-infection and retained the same level of expression for the remainder of the time points assessed. Many of the significant genes that had a positive log-fold change comparing week two vs. uninfected were proinflammatory genes, including *Gbp2* (guanylate binding protein 2), *Ccr5*, and *Ctss* (cathepsin S), and were also significantly different in week two vs. uninfected in MacMono.2, MacMono.3, and MacMono.4 sub-clusters (Figure 2D). Additionally, genes that were significantly downregulated between week two and uninfected were similar across sub-clusters, indicating that despite the different cluster-defining genes, the macrophage/monocyte sub-clusters respond to *B. burgdorferi* infection similarly. Given the significantly increased expression of several cytokine receptors (*Ccr2*, *Ccr5*, *Ccr1*; Figure 2D), we reanalyzed previously published cytokine array data[12] to assess the differences in key cytokines across uninfected, week two, and week four post-infection. We found that the production of the ligands for these cytokine receptors, specifically CCL2 and CCL3, were significantly increased in ankle joints of mice at week two post-infection compared to uninfected, and that levels of these cytokines returned to baseline at week four post-infection (Figure 2E). Together, these data provide validation that there is an initial burst of inflammation that is resolved shortly thereafter (Figure S2F), which occurs before the clinical resolution of arthritis and joint swelling between six and eight weeks post-infection.[4,7,8,13]

Using the fold changes generated through pseudobulk differential expression, we next performed GSEA for the MacMono.1 sub-cluster, using the comparison between week two and uninfected (Figure 2F; Table S3). Many of the pathways that had a positive enrichment score (were enriched in week two compared to uninfected) were inflammatory pathways that represented some change in the immune response, including the pathway "Response to Bacterium" (Figure 2G). Many of the pathways that were negatively enriched were associated with basic cellular functions, including cellular respiration (Figure 2H) and oxidative phosphorylation, suggesting that upon *B. burgdorferi* infection, macrophages and monocytes in the ankle joint switch from a resting/homeostatic state to a pro-inflammatory state.

## B cells and neutrophils undergo changes in sub-cluster composition following infection

After identifying the transcriptional changes occurring in the macrophage and monocyte sub-clusters, we re-clustered B cells which were the next largest immune cell subset recovered. Following doublet removal (Figures S3A and S3B), we identified six distinct B cell sub-clusters (Figure S3C). Among others, sub-clusters included an MHC class II high cluster (*H2-Aa, H2-Ab1*), and a cycling cluster (*Mki67, Pclaf*) (Figure S3D; Table S1). When we performed pseudobulk differential expression analysis, few genes of interest were found to change significantly over time within sub-clusters (Table S4). Despite having few transcriptional changes, B cell gene expression did peak at week two (Figure S3G). However, we observed a striking difference in the sub-cluster composition of B cells (Figures S3E and S3F), especially comparing uninfected mice to week two mice. For example, by week two, the cycling B cell cluster (Bcell.4) had undergone a rapid expansion (uninfected = 7%; week two = 30%). These results suggested that although within sub-clusters, transcriptional changes were few over time, the B cell population shifted in its makeup following infection.

Given the fragility of granulocytes and their difficulty in being captured by scRNA-seq technology,[14] we were surprised to discover many neutrophils were successfully recovered from the ankle joint. In fact, neutrophils were the third most abundant immune cell subset. Re-clustering of the neutrophil population and doublet removal (Figures S4A and S4B) yielded six new sub-clusters of neutrophils (Figure S4C). These sub-clusters had varying levels of expression of inflammatory genes including *Cxcl2, Il1b, Ngp* (neutrophilic granule protein), *Mpo* (myeloperoxidase), and *Elane* (neutrophil elastase) (Figure S4D; Table S1). Similar to B cells, we saw a pronounced alteration in the composition of clusters over time, especially comparing uninfected mice to week two (Figures S4E and S4F). Even beyond week two, there was an expansion at weeks six and eight of Neut.1, which had high expression of *Cxcl2*, *Tnfaip2, Il1b*, and *Csf1* (M-CSF). When performing pseudobulk differential expression analysis, there were very few transcriptional changes occurring over time within sub-clusters, as we also discovered with B cells (Table S5), though there was a peak in transcriptional activity at week two that subsided over time (Figure S4G). Although by pseudobulk differential expression we saw few transcriptional changes of note, using a non-pseudobulk approach (i.e., Wilcoxon rank-sum test), we saw slight changes in several important immune-related genes including *Cd274* (PD-L1), *B2m*, *Csf1*, and *Cxcl3* in certain sub-clusters when compared to uninfected samples (Figure S4H).

## $CD4^+$ T cells form the dominant T cell response against *Borrelia burgdorferi* infection

Although T cells comprised one of the smaller fractions of the immune cells captured by single-cell RNA sequencing, we assessed heterogeneity within the T cell response. We re-clustered T cells into four new sub-clusters (Figure 3A) following doublet removal (Figures S5A–S5D). Based on cluster-defining genes, Tcell.1 sub-cluster was likely $CD8^+$ T cells, Tcell.2 comprised of $CD4^+$ T cells, Tcell.3 comprised of a mixture of γδ and NKT cells, and Tcell.4 were cycling T cells (Figures 3B and 3C; Table S1). Pseudobulk differential expression analysis revealed that Tcell.2 ($CD4^+$ cells) upregulated several key genes involved in mounting an immune response including *Ifng* and several T cell

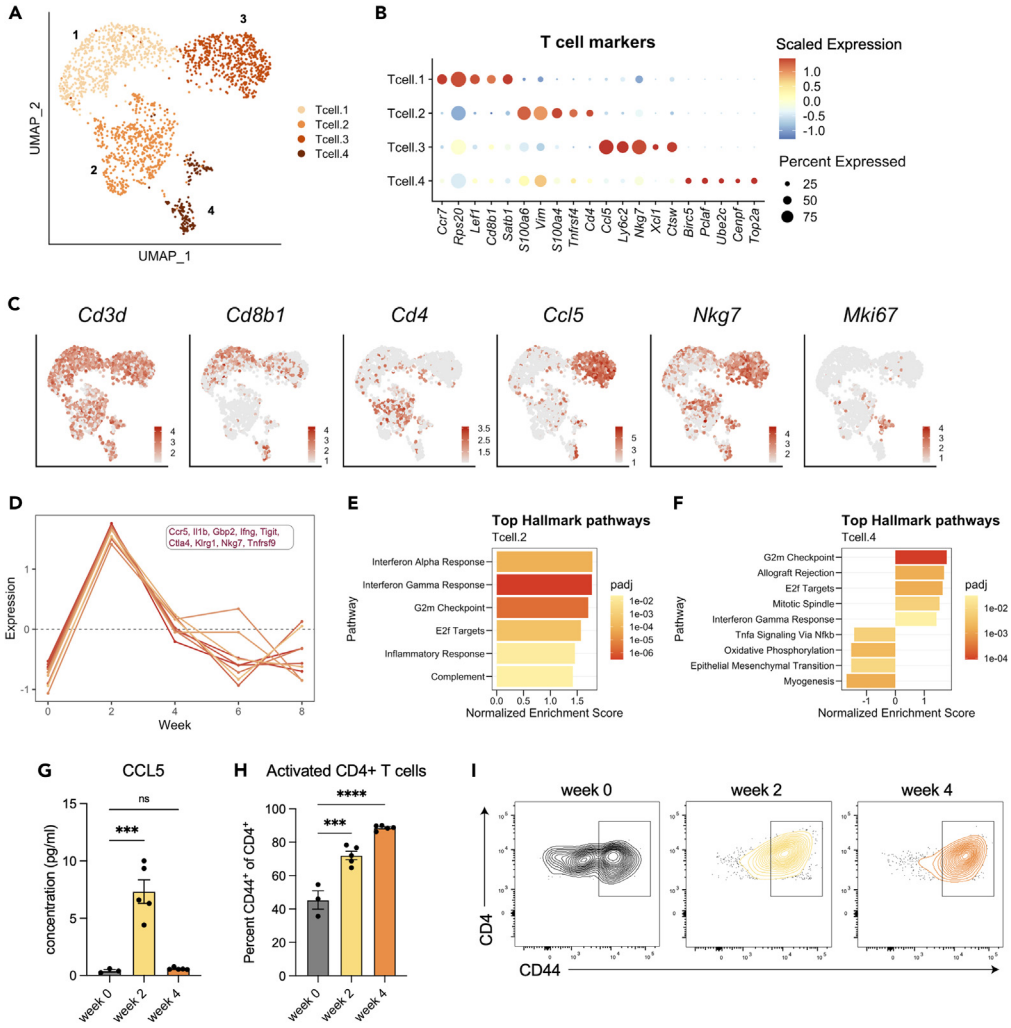


**Figure 3. T cell sub-clustering shows an activated CD4$^+$ response by week two of infection**

(A) T cells were re-clustered to exclude doublets and visualized using a UMAP revealing 4 distinct sub-clusters with B) expression of distinct cluster-defining genes.

(C) Expression of canonical markers across the T cell sub-clusters.

(D) Pseudobulk analysis of T cell.2 sub-cluster showing some of the top significant T cell activation genes changing over time.

(E) Hallmark pathway GSEA for week 0 vs. week 2 within T cell.2 and F) T cell.4 sub-clusters.

(G) Re-analyzed cytokine array of CCL5 production in ankle joints of mice over time from Helble et al.[12]

(H) Ankle joints of mice were harvested at the indicated time points and processed for flow cytometry. Activated CD4$^+$ T cells were determined as the percentage of CD44$^+$ cells from live → CD3$^+$ CD45$^+$ → CD4$^+$ cells. For G) and H), data were analyzed using ordinary one-way analysis of variance (ANOVA) with Dunnett's multiple comparisons test and are representative of at least 3 mice per group and are represented as the mean ± SEM; ***p < 0.001, and ****p < 0.0001.

(I) Representative flow plots showing CD44 changes over the different time points assessed.

See also Figure S5, and Tables S3 and S6.

activation genes including *Tigit, Ctla4*, and *Tnfrsf9* (4-1BB) (Figure 3D; Table S6). There was also abundant *Nkg7* and *Klrg1* expressed (Figure 3D), which suggested a cytotoxic or exhausted CD4 response.[12,15] However, similar to macrophages and monocytes, expression of these genes peaked at week two and returned close to uninfected levels of expression by week six or eight (Figure S5E).

Gene set enrichment analysis of genes significantly changed between uninfected and week two revealed "Interferon Alpha" and "Interferon Gamma" responses were greatly elevated in Tcell.2 (Figure 3E; Table S3). In the Tcell.4 sub-cluster, gene set enrichment analysis revealed an enrichment in the "G2m Checkpoint," which suggested this cycling cluster was undergoing even more proliferation (Figure 3F). Indeed, sub-cluster composition showed an increase in Tcell.4 levels, peaking at week four (Figures S5C and S5D). Tcell.2 levels were also slightly increased over time (Figures S5C and S5D). Pseudobulk differential expression analysis was not possible for Tcell.1 and Tcell.3 sub-clusters given the lack of cells captured from the CD45$^-$ enriched population. However, even through non-pseudobulk Wilcox rank-sum differential gene expression analyses, few genes changed in these sub-clusters over time.

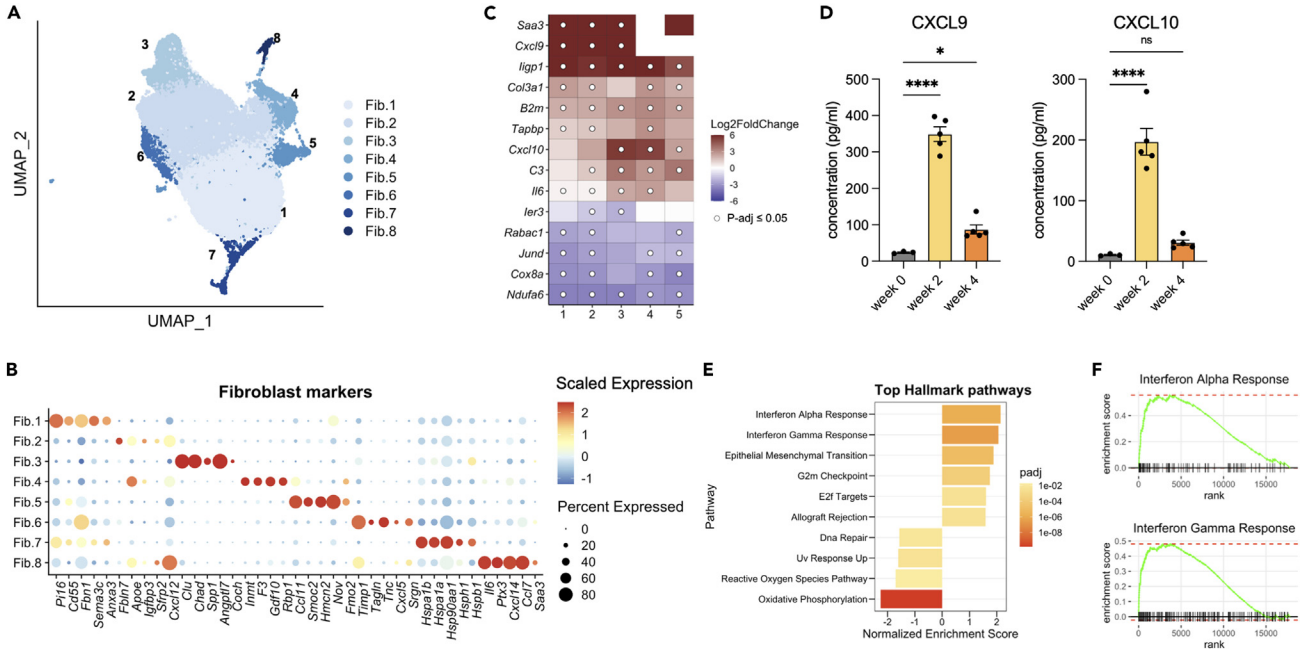


**Figure 4. Heterogeneous fibroblast clusters develop a homogeneous inflammatory response to *B. burgdorferi***

(A) Re-clustered UMAP of fibroblast subsets.

(B) Cluster-defining genes of the 8 different fibroblast sub-clusters.

(C) Pseudobulk analysis was performed over time for each sub-cluster. Heatmap depicts many of the genes significantly changed over time which were shared across clusters; log2 fold change for week 2 vs. week 0.

(D) Re-analyzed cytokine array of CXCL9 and CXCL10 production in ankle joints of mice over time from Helble et al.[12] Data were analyzed using ordinary one-way analysis of variance (ANOVA) with Dunnett's multiple comparisons test and are representative of at least 3 mice per group and are represented as the mean ± SEM; *p < 0.05, and ****p < 0.0001.

(E) GSEA of week 0 vs. week 2 for Fib.1 sub-cluster.

(F) Top GSEA enrichment plots from E).

See also Figure S6, and Tables S3 and S7.

Given the significant changes in *Ccr5* expression by pseudobulk differential expression analysis (Figure 3D), we reassessed our previously published cytokine array[12] for changes over time in its cognate ligand, CCL5. We found that CCL5 production mirrored *Ccr5* expression, as it was significantly increased in week two post-infection compared to uninfected mice and that by week four post-infection, CCL5 levels had returned to baseline (Figure 3G). To assess if the increase in activated $CD4^+$ T cells by scRNA-seq could be recapitulated, we performed flow cytometry on the ankle joints of mice at week two and four post-infection compared to uninfected. Although *Cd44* was not significantly changed as assessed by pseudobulk differential gene analysis, it is a common marker for T cell activation by flow cytometry and was thus used as a proxy. We found that the percentage of $CD44^+$ $CD4^+$ T cells was significantly increased at week two compared to uninfected mice (Figures 3H and 3I). We also observed that at week four post-infection, the levels of $CD44^+$ $CD4^+$ T cells were still elevated above uninfected controls.

## Fibroblast and synoviocyte populations express pro-inflammatory immune genes following *B. burgdorferi* infection

Fibroblasts were the predominant cell population in the ankle joint (Figure 1B) and have been previously shown to play a role in Lyme arthritis.[16,17] As with other cell clusters, the fibroblasts were initially re-clustered to remove doublets (Figures S6A and S6B), then re-clustered to reveal eight total fibroblast sub-clusters that were comprised of two large fibroblast sub-clusters (Fib.1 and Fib.2) and six transcriptionally distinct smaller sub-clusters (Figure 4A) that were represented across the time points (Figures S6C and S6D). The two largest sub-clusters differed based on their expression of *Pi16* (peptidase inhibitor 16), *Cd55*, *Fbln7* (fibulin 7) and *Apoe* (apolipoprotein E) (Figure 4B). When we performed pseudobulk differential expression analysis, we found that many of the transcriptional changes across clusters occurred between uninfected and week two, similar to what we had observed with the various immune cell populations (Figure S6E; Table S7). As with the immune cell clusters, many of the genes that were significantly different between uninfected and week two in Fib.1 were also significantly different or held similar trends across other sub-clusters including Fib.2, Fib.3, Fib.4 and Fib.5 (Figure 4C). Many of the genes that were significantly enriched in week two vs. uninfected included pro-inflammatory genes, such as *Cxcl9*, *Cxcl10*, *B2m* (β2 microglobulin), and *Il6* (Figure 4C). Given the significant expression of *Cxcl9* and *Cxcl10*, we reassessed our previously published cytokine array for changes in CXCL9 and CXCL10 production over time.[12] We found that both CXCL9 and CXCL10 production were significantly increased at week two post-infection compared to uninfected, and that these levels dropped at week four post-infection (Figure 4D).

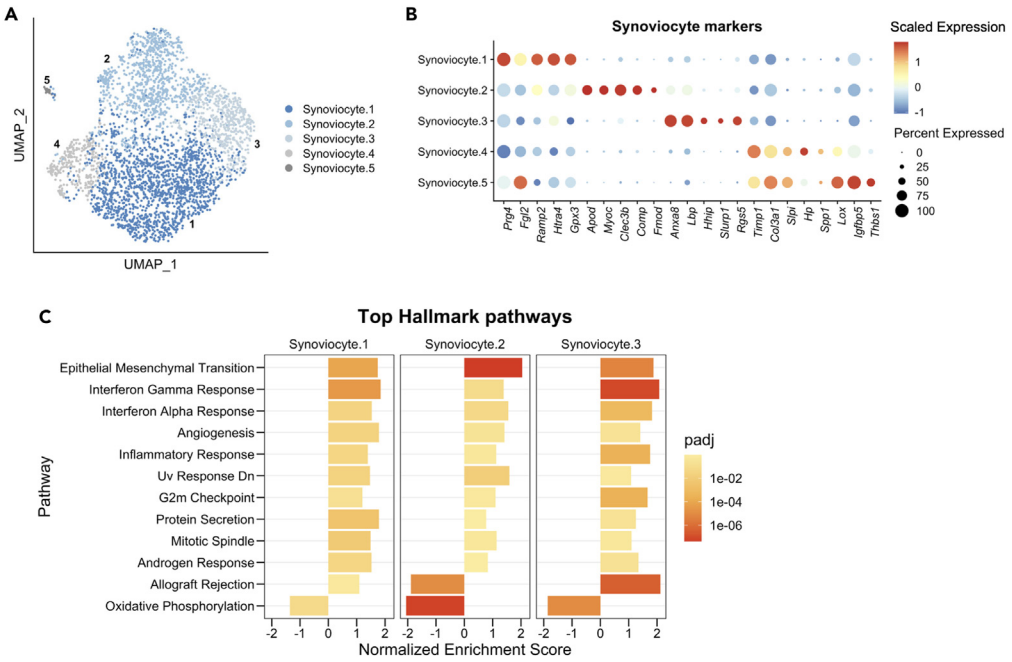


**Figure 5. Distinct synoviocyte sub-groups respond to infection in a similar manner**

(A) Sub-clustering of synoviocytes revealed 5 distinct groups, with B) unique cluster-defining gene expression.

(C) Hallmark GSEA comparing week 0 to week 2 for each synoviocyte sub-cluster.

See also Figure S6, and Tables S3 and S8.

When we performed GSEA on ranked genes comparing week two to uninfected in the Fib.1 sub-cluster, we found that the top two pathways that had a significantly positive enrichment score were the "Interferon Alpha Response" and the "Interferon Gamma Response" (Figures 4E and 4F; Table S3), while pathways with a significantly negative enrichment score were associated with cellular homeostasis. These findings suggest that upon *B. burgdorferi* infection, fibroblasts switch to a pro-inflammatory immune cell-like phenotype.

While synoviocytes are similar to fibroblasts, we found that they were a distinct population (Figure 1B). While lower in abundance than fibroblasts, during *B. burgdorferi* infection, synoviocytes have been reported to be involved in inducing Lyme arthritis in both mice and humans.[16,17] We found that synoviocytes had both high expression of the fibroblast cluster defining gene *Col1a1* (collagen type 1) as well as *Prg4* (proteoglycan 4), a common synoviocyte marker which helped to separate these cells from the fibroblasts.[18] After fibroblasts, synoviocytes were the second largest non-immune cell population found in the ankle joint. Synoviocytes were re-clustered to remove doublets (Figures S6F and S6G) and then re-clustered into five transcriptionally distinct sub-clusters (Figures 5A and 5B; Table S1) Similar to the B cell and neutrophil populations, there were alterations in the composition of these clusters between the uninfected and week two time points (Figures S6H and S6I). For example, we found that at week two post-infection, there was a decrease in abundance in the Synovocyte.2 sub-cluster that coincided with an increase in both Synoviocyte.3 and Synoviocyte.5 sub-clusters. Pseudobulk differential expression analysis of synoviocyte sub-clusters revealed there were large differences between uninfected and week two post-infection, consistent with the other cell populations (Figure S6J; Table S8). GSEA of the synoviocyte sub-clusters between uninfected and week two post-infection revealed similarities in pathways across the three largest synoviocytes populations (Figure 5C; Table S3). As with the fibroblasts, two of the top pathways for synoviocytes with a positive enrichment score were the "Interferon Gamma Response" and the "Interferon Alpha Response," suggesting that synoviocytes, like fibroblasts, become pro-inflammatory upon *B. burgdorferi* infection.

## Prediction of cell-cell communication

For all major clusters analyzed, peak transcriptional changes occurred between the uninfected and week two timepoints. Because of this, we opted to perform cell-cell communication prediction analysis between these two timepoints from our previously generated pseudobulk differential analysis (Table S9). Of the sub-populations analyzed, we found a high number of predicted interactions to occur within each main cell type. For example, distinct fibroblasts sub-clusters were found to interact with each other, as did MacMono sub-clusters with one another (Figure 6A). We also found between-cell-type interactions, most predominantly that of MacMono sub-clusters with predicted interactions with synoviocytes and fibroblasts (Figure 6A).

We further delineated the cell-cell communication prediction analysis to identify particular sub-clusters that might be responsible for cytokine/chemokine receptor-ligand interactions that we had previously identified using pseudobulk differential expression data and validated using ELISA. In particular, we looked at *Ccr5-Ccl2*, *Ccr5-Ccl3*, *Tlr4-Cxcl10*, *Ccr2-Ccl2*, *Ccr1-Ccl2*, and *Ccr1-Ccr3* interactions (Figure 6B). Again,

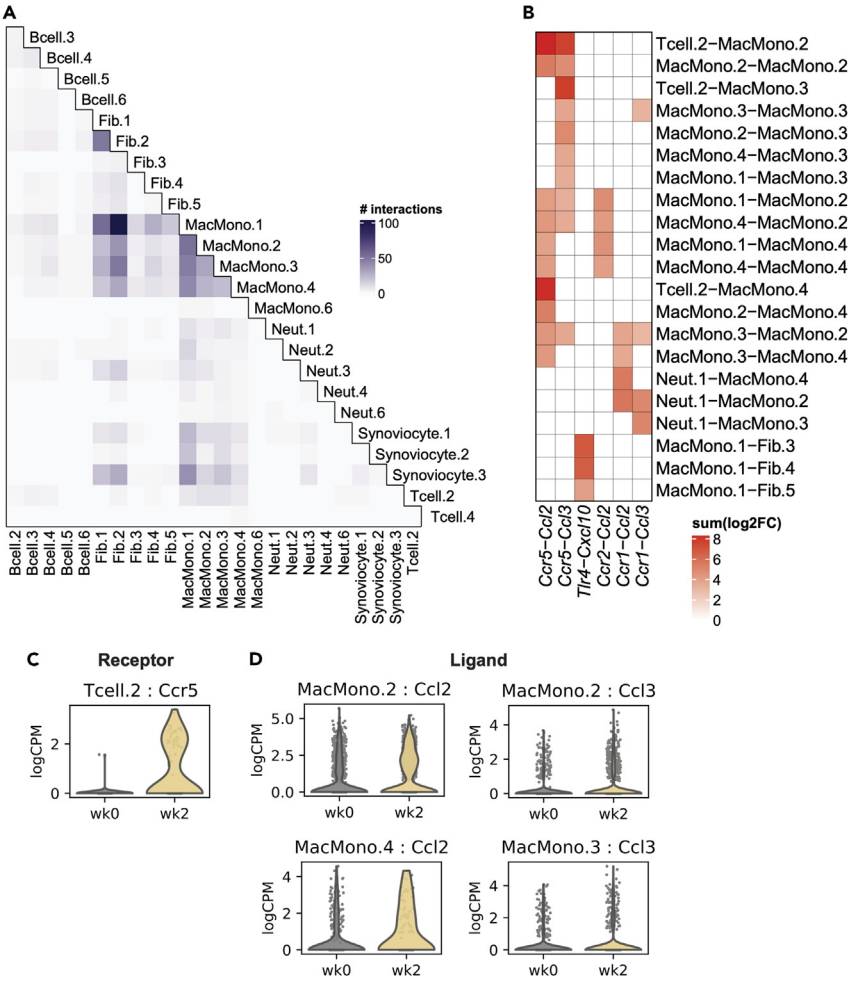


**Figure 6. Predicted cell-cell interactions in the ankle of infected mice**

(A) Total number of significant receptor-ligand interactions between week 0 and week 2 for separate sub-clusters.

(B) Specific significant receptor-ligand interactions with ligand protein data validation, both between and among sub-clusters. Scale indicates the sum of receptor and ligand log2-fold change between uninfected and week 2.

(C and D) Per-cell expression data of select interactions from B).

See also Table S9.

we found that sub-clusters might not only interact within the same sub-cluster (e.g., MacMono.3 *Ccl3* with MacMono.3 *Ccr5*), but also between sub-clusters of the same cell type (e.g., MacMono.2 *Ccl2* with MacMono.1 *Ccr2)* and between sub-clusters of differing cell types (e.g., MacMono.4 *Ccl2* with Tcell.2 *Ccr5*) (Figure 6B). MacMono clusters formed the dominate interactions among themselves and with T cells, fibroblasts, and neutrophils (Figure 6B). *Ccr5* was one of the highest upregulated genes in Tcell.2 between uninfected and week two timepoints (Figures 3D and 6C), and its corresponding ligands, *Ccl2* and *Ccl3* were significantly upregulated in multiple MacMono sub-clusters (Figure 6D). Together, these data indicate that there are likely many important cell-cell interactions that occur in the mouse ankle joint following *B. burgdorferi* infection, with macrophages playing a central role in coordinating the immune response.

## DISCUSSION

Technologies such as single-cell RNA-seq allow us to generate new insights into the evolution of the interactions between the immune system and pathogens such as *B. burgdorferi*. Previous studies using microscopy, the examination of protein expression, and/or gene transcripts from infected joint tissues from humans and mice have clearly shown the inflammatory nature of Lyme arthritis. However, little is understood about how the cellular composition evolves through the infection and which cells are critical for contribution to the inflammatory milieu. We performed single-cell RNA sequencing of C57BL/6 mouse ankle joints over time to trace the changes in the joint environment during peak and resolving infection in an animal model of infection. By capturing specific time points over the course of infection, ranging from uninfected mice up to week eight post-infection, we were able to analyze different stages in initial infection, stabilization, and ultimately resolution. In C57BL/6

mice, *B. burgdorferi* reach the joints early, typically under a week, and bacterial load continues to increase over the first four weeks after infection.[19–21] Pathologic inflammation is typically seen by two weeks following infection and continues to increase until week four, and it resolves by six to eight weeks following infection despite the continued presence of bacteria.[4,7,8,13]

Using scRNA-seq, we were able to determine cellular composition in infected mouse joints over time. Not surprisingly, macrophages/monocytes, T cells, B cells and neutrophils were the predominant immune cells in the joint. Neutrophils in particular have previously been identified as an important cell type in the joints during murine and human Lyme arthritis.[22] Although we observed expansions in different neutrophil sub-clusters over time, there were few transcriptional changes that occurred, likely reflecting that *B. burgdorferi* infection does not necessarily induce transcriptional changes of neutrophils but rather cellular accumulation. While B cells have been reported to be important for adaptive immunity to *B. burgdorferi*,[23] we also observed very few changes to B cell sub-clusters over time. Although we did not conduct B cell receptor (BCR) sequencing in tandem with our single cell due to pooling samples from multiple mice per timepoint, it is possible that by sequencing cells from individual mice separately and conducting BCR-seq, we may have observed the accumulation of certain B cell clones over time, potentially indicating *B. burgdorferi* specific B cells. Understanding how clonality changes over time may also aid in determining whether specific B cell populations are more or less likely to contribute to pathology, as some anti-*B. burgdorferi* antibodies are maintained for long periods of time.[13,24] Furthermore, several *B. burgdorferi* lipoproteins have demonstrated B cell mitogenic properties,[25] and it is unclear what role this phenomenon may play in limited transcriptional changes over time following infection.

In contrast to neutrophils and B cells, we saw a significant evolution of macrophage/monocyte gene expression at different timepoints of infection despite the distribution of the macrophage/monocyte sub-clusters remaining relatively stable over time. Our pseudobulk differential expression results indicated that changes in gene expression over time remained consistent across multiple macrophage/monocyte sub-clusters, even though these sub-clusters had differences in their M1/M2 categorization, which have been reported to influence inflammation differently. We found using cell-cell communication prediction analysis that macrophage/monocytes appeared to be highly connected both to themselves and other cell types, including non-hematopoetic cells such as synoviocytes and fibroblasts. The role of macrophages versus synoviocytes in driving the inflammatory response to *B. burgdorferi* has long been debated.[16,17,26] Our data suggests that macrophages are likely at the center of coordinating the inflammatory response to *B. burgdorferi*. However, we found that macrophages, synoviocytes and fibroblasts likely all contribute to the type I IFN (IFN-α and IFN-β) and type II IFN (IFN-γ) response pathways following infection. Interestingly, the type I IFN response has been shown to play a critical role in murine Lyme arthritis development in C3H but not C57BL/6 mice.[16,27,28] While C57BL/6 mice have less inflammation and therefore a likely diminished role for type I IFN in disease development, the sensitivity of scRNA-seq shows a clear upregulation of this pathway in several cell types. Type I IFN responses have been recently correlated with not only human erythema migrans (typically one of the first manifestations of Lyme disease),[5,29] but also Lyme neuroborreliosis in both humans and C3H mice.[30,31] The type I IFN pathway is clearly a central component of inflammation associated with Lyme disease, but the correlations between the type I IFN responses in C57BL/6 mice and humans are still unclear.[32]

IFNγ has been shown to play a role during *B. burgdorferi* infection in both mice and in humans, however its role in pathogenesis is uncertain. IFNγ-deficient C3H mice were found to have modest increases in ankle swelling compared to their wild-type counterparts,[33] though conversely, treatment with anti-IFNγ antibodies reduced C3H joint swelling.[34] In C57BL/6 mice, knockout of IL-10 can induce ankle swelling during infection, with anti-IFNγ antibodies reducing swelling to wild-type levels, suggesting IFNγ may drive arthritis in this IL-$10^{-/-}$ model.[35] IFNγ may also reduce the severity of Lyme carditis through several mechanisms, including promoting macrophage phagocytosis of bacteria.[36] The abundance of macrophages present in our dataset and the enrichment in the "phagocytosis" GO pathway suggests this could be happening in the joints of these mice in response to IFNγ. In humans with Lyme arthritis, there is elevation of IFNγ in synovial fluid, compared to patients with osteoarthritis.[17] In addition, synovial tissue from patients with Lyme arthritis has been found to express lower levels of tissue repair genes.[6] Like many of the other cell types, synoviocytes and fibroblasts captured in our dataset had an elevated IFNγ-response signature at week two post-infection, suggesting that these non-hematopoietic cells switch to a pro-inflammatory immune cell-like phenotype following *B. burgdorferi* infection. The process by which synoviocytes and fibroblasts become inflammatory has been shown to occur in response to IFNγ signaling in both Lyme arthritis and rheumatoid arthritis,[17,37,38] suggesting that this might be a central axis in joint inflammation across indications. Though wild-type C57BL/6 mice ultimately resolve infection and have little lasting joint inflammation, it is possible that IFNγ could prevent the tissue repair by synoviocytes, fibroblasts, and macrophages in other mouse models and in humans. IFNγ, which is a common Th1 cytokine, was expressed by the Tcell.2 sub-cluster. The balance between Th1 and Th2 responses may ultimately influence the outcome of infection and any lasting Lyme complications.[17,39,40]

We found that for all cell types, the majority of transcriptional changes peaked at two weeks of infection. In particular, macrophage/monocyte gene expression returned to near baseline by week four, which was unexpected given that bacterial burden in the joints remains high at four weeks post-infection.[12] This suggests that the macrophages may have become less responsive to stimulation by *B. burgdorferi* over time. We have previously shown using an *in vitro* model of repeated stimulation that macrophages develop immune memory that dampens subsequent inflammatory responses upon repeated encounters with *B. burgdorferi*.[41] This may be a protective mechanism in cases where the activation of the immune system is more damaging than the infection. Similarly, T cells may exhibit an exhausted phenotype with repeated stimulation that can dampen inflammatory signaling. In particular, we have previously demonstrated that the T cell exhaustion pathway PD-1/PD-L1 is upregulated during infection and may play a role in the C57BL/6 resolution of inflammation.[12] Using scRNA-seq, we found that other exhaustion markers, such as *Tigit* and *Ctla4* are upregulated at week two post-infection, further suggesting that the long-term infection of *B. burgdorferi* can impact multiple cell populations.

In wild mice, *B. burgdorferi* is treated by the immune system as a commensal organism that elicits little to no inflammatory response despite continued presence of the bacteria within the animal. While humans and inbred mice do develop an inflammatory response including arthritis, natural history studies (done in humans before the discovery of the efficacy of antibiotics) found that these responses resolve spontaneously over time without antibiotic treatment. Our data similarly suggest that the peak in transcriptional changes quickly resolves fairly early in infection. It seems likely that a similar phenomenon occurs in humans. With the advent of antibiotic therapy for Lyme disease, most symptoms of inflammation are resolved quickly with treatment. However, in a small subset of humans with Lyme arthritis, joint inflammation can persist even after antibiotic therapy.[5] It has been shown that *B. burgdorferi* membrane components can be retained for long periods of time and may continue to stimulate a response.[24] Why it does so in only a subset of patients has been a mystery. Our studies provide insight into the natural evolution of the immunologic response to *B. burgdorferi* and may provide clues as to what may cause pathological inflammation in certain predisposed patients.

### Limitations of the study

Although murine and human Lyme arthritis share many similarities, there are known differences both in the course of the disease and some of the inflammatory cytokines expressed. Furthermore, each mouse strain responds differently to *B. burgdorferi*, and it has not yet been established which strain of mice may more closely mimic human disease. Because C57BL/6 mice have milder joint pathology compared to some other mouse strains, it is unknown if the transcriptional changes we observed at week two post-infection reflect a general response to *B. burgdorferi* in the tissue or are strain and species specific. Additionally, our validation efforts were mainly focused on cytokine/chemokine production in the ankle joint where it was possible to compare our results with prior work. Future work should aim to further dissect how certain cell types/sub-populations interact across different pathways, how joint pathology at different time points correlates with the transcriptional changes we observed, and ultimately how these differ across mouse strain and in human joint tissue.

## STAR★METHODS

Detailed methods are provided in the online version of this paper and include the following:

- KEY RESOURCES TABLE
- RESOURCE AVAILABILITY
  - Lead contact
  - Materials availability
  - Data and code availability
- EXPERIMENTAL MODEL AND STUDY PARTICIPANT DETAILS
  - Mice
  - Bacteria
- METHOD DETAILS
  - Infection of mice and preparation of tissue
  - Single cell RNA library preparation and sequencing
  - Single-cell RNA sequencing pre-processing
  - Clustering analysis of single cell data
  - Differential gene expression analysis
  - Gene set enrichment analysis
  - Cell-cell communication analysis
  - Cytokine assessment
  - Flow cytometry analysis
  - Visualization
- QUANTIFICATION AND STATISTICAL ANALYSIS

## SUPPLEMENTAL INFORMATION

Supplemental information can be found online at https://doi.org/10.1016/j.isci.2023.108217.

## ACKNOWLEDGMENTS

The authors thank Dr. Tanja Petnicki-Ocwieja and Dr. Jeffrey Bourgeois for their helpful discussions. The project was supported by the National Institutes of Health grants R01AI150157 and R01AI131656 to LTH and the Harvard Fairbairn Family Lyme Disease Research Initiative grant to LTH.

## AUTHOR CONTRIBUTIONS

J.D.H., J.E.M., and L.T.H. designed the study. J.D.H. and J.E.M. performed *in vivo* set up and cell isolation for scRNA-seq. A.J.T., B.Y.A., and A.C.V assisted with single cell library preparation. J.D.H., M.J.W., and N.P.S. conducted scRNA-seq analysis, and J.D.H. performed cytokine and flow cytometry experiments. J.D.H., M.J.W., and L.T.H. wrote the article with input from all authors.

## DECLARATION OF INTERESTS

L.T.H. receives support for contract research services through Tufts University from companies including Moderna, Sanofi, Tarsus, and Mass-biologics for vaccine and drug development unrelated to the content of this article.

Received: July 20, 2023
Revised: September 6, 2023
Accepted: October 11, 2023
Published: October 14, 2023

## REFERENCES

1. Radolf, J.D., Caimano, M.J., Stevenson, B., and Hu, L.T. (2012). Of ticks, mice and men: Understanding the dual-host lifestyle of Lyme disease spirochaetes. Nat. Rev. Microbiol. *10*, 87–99. https://doi.org/10.1038/nrmicro2714.
2. Kugeler, K.J., Schwartz, A.M., Delorey, M.J., Mead, P.S., and Hinckley, A.F. (2021). Estimating the frequency of Lyme disease diagnoses, United States, 2010-2018. Emerg. Infect. Dis. *27*, 616–619.
3. Schwartz, A.M., Kugeler, K.J., Nelson, C.A., Marx, G.E., and Hinckley, A.F. (2021). Use of commercial claims data for evaluating trends in Lyme disease diagnoses, United States, 2010-2018. Emerg. Infect. Dis. *27*, 499–507. https://doi.org/10.3201/eid2702.202728.
4. Lochhead, R.B., Strle, K., Arvikar, S.L., Weis, J.J., and Steere, A.C. (2021). Lyme arthritis: linking infection, inflammation and autoimmunity. Nat. Rev. Rheumatol. *17*, 449–461. https://doi.org/10.1038/s41584-021-00648-5.
5. Steere, A.C., Strle, F., Wormser, G.P., Hu, L.T., Branda, J.A., Hovius, J.W.R., Li, X., and Mead, P.S. (2016). Lyme borreliosis. Nat. Rev. Dis. Primers *2*, 16090. https://doi.org/10.1038/nrdp.2016.90.
6. Lochhead, R.B., Arvikar, S.L., Aversa, J.M., Sadreyev, R.I., Strle, K., and Steere, A.C. (2019). Robust interferon signature and suppressed tissue repair gene expression in synovial tissue from patients with postinfectious, Borrelia burgdorferi-induced Lyme arthritis. Cell Microbiol. *21*, e12954. https://doi.org/10.1111/cmi.12954.
7. Barthold, S.W. (1995). Animal models for Lyme disease. Lab. Invest. *72*, 127–130.
8. Ma, Y., Seiler, K.P., Eichwald, E.J., Weis, J.H., Teuscher, C., and Weis, J.J. (1998). Distinct characteristics of resistance to Borrelia burgdorferi induced arthritis in C57BL/6N mice. Infect. Immun. *66*, 161–168. https://doi.org/10.1128/iai.66.1.161-168.1998.
9. Bramwell, K.K.C., Ma, Y., Weis, J.H., Chen, X., Zachary, J.F., Teuscher, C., and Weis, J.J. (2014). Lysosomal beta-glucuronidase regulates Lyme and rheumatoid arthritis severity. J. Clin. Invest. *124*, 311–320. https://doi.org/10.1172/JCI72339.
10. Steere, A.C. (1997). Diagnosis and treatment of lyme arthritis. Med. Clin. North Am. *81*, 179–194. https://doi.org/10.1016/S0025-7125(05)70510-1.
11. Li, C., Menoret, A., Farragher, C., Ouyang, Z., Bonin, C., Holvoet, P., Vella, A.T., and Zhou, B. (2019). Single-cell transcriptomics-based MacSpectrum reveals macrophage activation signatures in diseases. JCI Insight *5*, e126453. https://doi.org/10.1172/jci.insight.126453.
12. Helble, J.D., McCarthy, J.E., Sawden, M., Starnbach, M.N., and Hu, L.T. (2022). The PD-1/PD-L1 pathway is induced during Borrelia burgdorferi infection and inhibits T cell joint infiltration without compromising bacterial clearance. PLoS Pathog. *18*, e1010903. https://doi.org/10.1371/journal.ppat.1010903.
13. Bockenstedt, L.K., Wooten, R.M., and Baumgarth, N. (2021). Immune response to Borrelia: Lessons from Lyme disease spirochetes. Curr. Issues Mol. Biol. *42*, 145–190. https://doi.org/10.21775/cimb.042.145.
14. Xue, R., Zhang, Q., Cao, Q., Kong, R., Xiang, X., Liu, H., Feng, M., Wang, F., Cheng, J., Li, Z., et al. (2022). Liver tumour immune microenvironment subtypes and neutrophil heterogeneity. Nature *612*, 141–147. https://doi.org/10.1038/s41586-022-05400-x.
15. Cachot, A., Bilous, M., Liu, Y.C., Li, X., Saillard, M., Cenerenti, M., Rockinger, G.A., Wyss, T., Guillaume, P., Schmidt, J., et al. (2021). Tumor-specific cytolytic CD4 T cells mediate immunity against human cancer. Sci. Adv. *7*, eabe3348. https://doi.org/10.1126/sciadv.abe3348.
16. Lochhead, R.B., Sonderegger, F.L., Ma, Y., Brewster, J.E., Cornwall, D., Maylor-Hagen, H., Miller, J.C., Zachary, J.F., Weis, J.H., and Weis, J.J. (2012). Endothelial Cells and Fibroblasts Amplify the Arthritogenic Type I IFN Response in Murine Lyme Disease and Are Major Sources of Chemokines in Borrelia burgdorferi-Infected Joint Tissue. J. Immunol. *189*, 2488–2501. https://doi.org/10.4049/jimmunol.1201095.
17. Lochhead, R.B., Ordoñez, D., Arvikar, S.L., Aversa, J.M., Oh, L.S., Heyworth, B., Sadreyev, R., Steere, A.C., and Strle, K. (2019). Interferon-gamma production in Lyme arthritis synovial tissue promotes differentiation of fibroblast-like synoviocytes into immune effector cells. Cell Microbiol. *21*, e12992. https://doi.org/10.1111/cmi.12992.
18. Wei, K., Korsunsky, I., Marshall, J.L., Gao, A., Watts, G.F.M., Major, T., Croft, A.P., Watts, J., Blazar, P.E., Lange, J.K., et al. (2020). Notch signalling drives synovial fibroblast identity and arthritis pathology. Nature *582*, 259–264. https://doi.org/10.1038/s41586-020-2222-z.
19. Crandall, H., Dunn, D.M., Ma, Y., Wooten, R.M., Zachary, J.F., Weis, J.H., Weiss, R.B., and Weis, J.J. (2006). Gene Expression Profiling Reveals Unique Pathways Associated with Differential Severity of Lyme Arthritis. J. Immunol. *177*, 7930–7942. https://doi.org/10.4049/jimmunol.177.11.7930.
20. Bolz, D.D., Sundsbak, R.S., Ma, Y., Akira, S., Kirschning, C.J., Zachary, J.F., Weis, J.H., and Weis, J.J. (2004). MyD88 Plays a Unique Role in Host Defense but Not Arthritis Development in Lyme Disease. J. Immunol. *173*, 2003–2010. https://doi.org/10.4049/jimmunol.173.3.2003.
21. Wang, X., Ma, Y., Weis, J.H., Zachary, J.F., Kirschning, C.J., and Weis, J.J. (2005). Relative contributions of innate and acquired host responses to bacterial control and arthritis development in lyme disease. Infect. Immun. *73*, 657–660. https://doi.org/10.1128/IAI.73.1.657-660.2005.
22. Barthold, S.W., and de Souza, M. (1995). Exacerbation of Lyme arthritis in beige mice. J. Infect. Dis. *172*, 778–784.
23. McKisic, M.D., and Barthold, S.W. (2000). T-cell-independent responses to Borrelia burgdorferi are critical for protective immunity and resolution of lyme disease. Infect. Immun. *68*, 5190–5197. https://doi.org/10.1128/IAI.68.9.5190-5197.2000.
24. Gwynne, P.J., Clendenen, L.H., Turk, S.P., Marques, A.R., and Hu, L.T. (2022). Antiphospholipid autoantibodies in Lyme disease arise after scavenging of host phospholipids by Borrelia burgdorferi. J. Clin. Invest. *132*, e152506. https://doi.org/10.1172/JCI152506.
25. Ma, Y., and Weis, J.J. (1993). Borrelia burgdorferi outer surface lipoproteins OspA and OspB possess B- cell mitogenic and cytokine-stimulatory properties. Infect. Immun. *61*, 3843–3853. https://doi.org/10.1128/iai.61.9.3843-3853.1993.
26. Bernard, Q., and Hu, L.T. (2020). Innate Immune Memory to Repeated Borrelia burgdorferi Exposure Correlates with Murine In Vivo Inflammatory Phenotypes. J. Immunol. *205*, 3383–3389. https://doi.org/10.4049/jimmunol.2000686.
27. Miller, J.C., Ma, Y., Bian, J., Sheehan, K.C.F., Zachary, J.F., Weis, J.H., Schreiber, R.D., and Weis, J.J. (2008). A Critical Role for Type I IFN in Arthritis Development following Borrelia burgdorferi Infection of Mice. J. Immunol. *181*, 8492–8503. https://doi.org/10.4049/jimmunol.181.12.8492.
28. Miller, J.C., Maylor-Hagen, H., Ma, Y., Weis, J.H., and Weis, J.J. (2010). The Lyme disease spirochete Borrelia burgdorferi utilizes multiple ligands, including RNA, for interferon regulatory factor 3-dependent induction of type I interferon-responsive genes. Infect. Immun. *78*, 3144–3153. https://doi.org/10.1128/IAI.01070-09.
29. Salazar, J.C., Pope, C.D., Sellati, T.J., Feder, H.M., Kiely, T.G., Dardick, K.R., Buckman, R.L., Moore, M.W., Caimano, M.J., Pope, J.G., et al. (2003). Coevolution of Markers of Innate and Adaptive Immunity in Skin and Peripheral Blood of Patients with Erythema Migrans. J. Immunol. *171*, 2660–2670. https://doi.org/10.4049/jimmunol.171.5.2660.
30. Casselli, T., Divan, A., Vomhof-DeKrey, E.E., Tourand, Y., Pecoraro, H.L., and Brissette, C.A. (2021). A murine model of Lyme disease demonstrates that Borrelia burgdorferi colonizes the dura mater and induces inflammation in the central nervous system.

PLoS Pathog. *17*, e1009256. https://doi.org/10.1371/JOURNAL.PPAT.1009256.

31. Hernández, S.A., Ogrinc, K., Korva, M., Kastrin, A., Bogovič, P., Rojko, T., Kelley, K.W., Weis, J.J., Strle, F., and Strle, K. (2023). Association of Persistent Symptoms after Lyme Neuroborreliosis and Increased Levels of Interferon-α in Blood. Emerg. Infect. Dis. *29*, 1091–1101. https://doi.org/10.3201/eid1906.221685.
32. Farris, L.C., Torres-Odio, S., Adams, L.G., West, A.P., and Hyde, J.A. (2023). Borrelia burgdorferi Engages Mammalian Type I IFN Responses via the cGAS–STING Pathway. J. Immunol. *210*, 1761–1770. https://doi.org/10.4049/JIMMUNOL.2200354.
33. Brown, C.R., and Reiner, S.L. (1999). Experimental Lyme arthritis in the absence of interleukin-4 or gamma interferon. Infect. Immun. *67*, 3329–3333. https://doi.org/10.1128/iai.67.7.3329-3333.1999.
34. Keane-Myers, A., and Nickell, S.P. (1995). Role of IL-4 and IFN-gamma in modulation of immunity to Borrelia burgdorferi in mice. J. Immunol. *155*, 2020–2028.
35. Sonderegger, F.L., Ma, Y., Maylor-Hagan, H., Brewster, J., Huang, X., Spangrude, G.J., Zachary, J.F., Weis, J.H., and Weis, J.J. (2012). Localized Production of IL-10 Suppresses Early Inflammatory Cell Infiltration and Subsequent Development of IFN-γ–Mediated Lyme Arthritis. J. Immunol. *188*, 1381–1393. https://doi.org/10.4049/jimmunol.1102359.
36. Olson, C.M., Bates, T.C., Izadi, H., Radolf, J.D., Huber, S.A., Boyson, J.E., and Anguita, J. (2009). Local Production of IFN-γ by Invariant NKT Cells Modulates Acute Lyme Carditis. J. Immunol. *182*, 3728–3734. https://doi.org/10.4049/jimmunol.0804111.
37. Sohn, C., Lee, A., Qiao, Y., Loupasakis, K., Ivashkiv, L.B., and Kalliolias, G.D. (2015). Prolonged tumor necrosis factor α primes fibroblast-like synoviocytes in a gene-specific manner by altering chromatin. Arthritis Rheumatol. *67*, 86–95. https://doi.org/10.1002/art.38871.
38. Korsunsky, I., Wei, K., Pohin, M., Kim, E.Y., Barone, F., Major, T., Taylor, E., Ravindran, R., Kemble, S., Watts, G.F.M., et al. (2022). Cross-tissue, single-cell stromal atlas identifies shared pathological fibroblast phenotypes in four chronic inflammatory diseases. Med *3*, 481–518.e14. https://doi.org/10.1016/j.medj.2022.05.002.
39. Gross, D.M., Steere, A.C., and Huber, B.T. (1998). T Helper 1 Response Is Dominant and Localized to the Synovial Fluid in Patients with Lyme Arthritis. J. Immunol. *160*, 1022–1028.
40. Vudattu, N.K., Strle, K., Steere, A.C., and Drouin, E.E. (2013). Dysregulation of CD4+CD25high T cells in the synovial fluid of patients with antibiotic-refractory lyme arthritis. Arthritis Rheum. *65*, 1643–1653. https://doi.org/10.1002/art.37910.
41. Petnicki-Ocwieja, T., DeFrancesco, A.S., Chung, E., Darcy, C.T., Bronson, R.T., Kobayashi, K.S., and Hu, L.T. (2011). Nod2 suppresses Borrelia burgdorferi mediated murine Lyme arthritis and carditis through the induction of tolerance. PLoS One *6*, e17414. https://doi.org/10.1371/journal.pone.0017414.
42. Petnicki-Ocwieja, T., Chung, E., Acosta, D.I., Ramos, L.T., Shin, O.S., Ghosh, S., Kobzik, L., Li, X., and Hu, L.T. (2013). TRIF mediates toll-like receptor 2-dependent inflammatory responses to Borrelia burgdorferi. Infect. Immun. *81*, 402–410. https://doi.org/10.1128/IAI.00890-12.
43. Stuart, T., Butler, A., Hoffman, P., Hafemeister, C., Papalexi, E., Mauck, W.M., Hao, Y., Stoeckius, M., Smibert, P., and Satija, R. (2019). Comprehensive integration of single-cell data. Cell *177*, 1888–1902.e21. https://doi.org/10.1016/J.CELL.2019.05.031.
44. Griffiths, J.A., Richard, A.C., Bach, K., Lun, A.T.L., and Marioni, J.C. (2018). Detection and removal of barcode swapping in single-cell RNA-seq data. Nat. Commun. *91*, 2667. https://doi.org/10.1038/s41467-018-05083-x.
45. Love, M.I., Huber, W., and Anders, S. (2014). Moderated estimation of fold change and dispersion for RNA-seq data with DESeq2. Genome Biol. *15*, 550. https://doi.org/10.1186/s13059-014-0550-8.
46. Liberzon, A., Birger, C., Thorvaldsdóttir, H., Ghandi, M., Mesirov, J.P., and Tamayo, P. (2015). The Molecular Signatures Database Hallmark Gene Set Collection. Cell Syst. *1*, 417–425. https://doi.org/10.1016/j.cels.2015.12.004.
47. Türei, D., Korcsmáros, T., and Saez-Rodriguez, J. (2016). OmniPath: Guidelines and gateway for literature-curated signaling pathway resources. Nat. Methods *13*, 966–967. https://doi.org/10.1038/nmeth.4077.
48. Gu, Z., Eils, R., and Schlesner, M. (2016). Complex heatmaps reveal patterns and correlations in multidimensional genomic data. Bioinformatics *32*, 2847–2849. https://doi.org/10.1093/bioinformatics/btw313.
49. Zheng, G.X.Y., Terry, J.M., Belgrader, P., Ryvkin, P., Bent, Z.W., Wilson, R., Ziraldo, S.B., Wheeler, T.D., McDermott, G.P., Zhu, J., et al. (2017). Massively parallel digital transcriptional profiling of single cells. Nat. Commun. *8*, 14049. https://doi.org/10.1038/ncomms14049.
50. Butler, A., Hoffman, P., Smibert, P., Papalexi, E., and Satija, R. (2018). Integrating single-cell transcriptomic data across different conditions, technologies, and species. Nat. Biotechnol. *36*, 411–420. https://doi.org/10.1038/NBT.4096.
51. Squair, J.W., Gautier, M., Kathe, C., Anderson, M.A., James, N.D., Hutson, T.H., Hudelle, R., Qaiser, T., Matson, K.J.E., Barraud, Q., et al. (2021). Confronting false discoveries in single-cell differential expression. Nat. Commun. *12*, 5692. https://doi.org/10.1038/s41467-021-25960-2.
52. Lun, A.T.L., Bach, K., and Marioni, J.C. (2016). Pooling across cells to normalize single-cell RNA sequencing data with many zero counts. Genome Biol. *17*, 75. https://doi.org/10.1186/s13059-016-0947-7.

## STAR★METHODS

### KEY RESOURCES TABLE

| REAGENT or RESOURCE | SOURCE | IDENTIFIER |
|---|---|---|
| **Antibodies** | | |
| Anti-mouse CD16/32 (clone S1700E) | BioLegend | Cat# 156603; RRID: AB_2783137 |
| Anti-mouse CD45 (clone 30-F11) | BioLegend | Cat# 103125; RRID: AB_493536 |
| Anti-mouse CD3 (clone 17A2) | BioLegend | Cat# 100241; RRID: AB_2563945 |
| Anti-mouse CD4 (clone GK1.5) | BioLegend | Cat# 100411; RRID: AB_312696 |
| Anti-mouse CD44 (clone IM7) | BioLegend | Cat# 103007; RRID: AB_493686 |
| LIVE/DEAD Fixable Aqua | Invitrogen | Cat# L34957 |
| **Bacterial and virus strains** | | |
| *Borrelia burgdorferi* B31 | Petnicki-Ocwieja et al.[42] | N/A |
| **Chemicals, peptides, and recombinant proteins** | | |
| Liberase TL | Millipore Sigma | Cat# 5401020001 |
| DNase I, RNase free | Thermo Fisher | Cat# EN0521 |
| RPMI 1640 | Corning | Cat# 10-040 CV |
| PBS | Gibco | Cat# 14190250 |
| FBS | R&D Systems | Cat# S11550H |
| $CaCl_2$ | Fisher Scientific | Cat# C79-500 |
| BSA | Rockland | Cat# BSA-50 |
| EDTA | Corning | Cat# 46-034-CI |
| **Critical commercial assays** | | |
| EasySep Dead Cell Removal (Annexin V) Kit | StemCell Technologies | Cat# 17899 |
| CD45 MicroBeads | Miltenyi Biotec | Cat# 130-052-301 |
| MiniMACS Separator | Miltenyi Biotec | Cat# 130-042-102 |
| Single Cell K Chip | 10x Genomics | Cat# 1000286 |
| Chromium Single Cell 5′ Library and Gel Bead Kit v2 | 10x Genomics | Cat# 1000263 |
| Library Construction Kit | 10x Genomics | Cat# 1000190 |
| Mouse Cytokine/Chemokine 31-Plex discovery assay | Eve Technologies | Cat# MD31 |
| **Deposited data** | | |
| Single cell RNA-sequencing raw data | This paper | NCBI GEO: GSE233850 |
| Source code | This paper | http://www.github.com/mjlwalsh/Bb_scRNAseq |
| **Experimental models: Organisms/strains** | | |
| Mouse: C57BL/6 mice | The Jackson Labs | Cat# 000664 |
| **Software and algorithms** | | |
| Cellranger v6.0.0 | 10x Genomics | http://www.10xgenomics.com/support/software/cell-ranger |
| Mm10 reference genome v3.0.0 | 10x Genomics | http://www.10xgenomics.com/support |
| R v4.1.1 | R Project | https://www.r-project.org/ |
| R Studio | Posit | https://posit.co/downloads/ |
| Seurat v4.0.5 | Stuart et al.[43] | https://satijalab.org/seurat/ |
| DropletUtils v1.14.2 | Griffiths et al.[44] | Bioconductor |

(*Continued on next page*)

*Continued*

| REAGENT or RESOURCE | SOURCE | IDENTIFIER |
|---|---|---|
| DESeq2 v1.38.2 | Love et al.[45] | Bioconductor |
| fgsea v1.24.0 | https://doi.org/10.1101/060012 | Bioconductor |
| Molecular Signature Hallmark gene set v7.2 | Liberzon et al.[46] | https://www.gsea-msigdb.org/ |
| GO gene set v7.5.1 | https://geneontology.org/ | https://geneontology.org/ |
| OmniPath v3.5.25 | Türei et al.[47] | Bioconductor |
| ComplexHeatmap v2.14.0 | Gu et al.[48] | Bioconductor |
| ggplot2 v3.4.0 | Hadley Wickham | https://ggplot2.tidyverse.org/ |
| Prism | GraphPad | https://www.graphpad.com/features |
| FlowJo v10.8.1 | TreeStar | https://www.flowjo.com/ |

## RESOURCE AVAILABILITY

### Lead contact

Further information and requests for resources and reagents should be directed to and will be fulfilled by the lead contact, Linden T. Hu (Linden.Hu@Tufts.edu).

### Materials availability

This study did not generate new unique reagents.

### Data and code availability

All raw and processed scRNA-seq data is deposited in the GEO database and are publicly available as of the date of publication. Accession numbers are listed in the key resources table. All original code has been deposited at GitHub and is publicly available as of the date of publication. The URL is listed in the key resources table. Any additional information required to reanalyze the data reported in this paper is available from the lead contact upon request.

## EXPERIMENTAL MODEL AND STUDY PARTICIPANT DETAILS

### Mice

Seven-week old female C57BL/6J mice were purchased from Jackson Laboratory (Bar Harbor, ME) and were group housed at Tufts University School of Medicine. All experiments were approved by the Institutional Animal Care and Use Committee at Tufts University (IACUC, Protocol #B2021-84). Mice were euthanized through CO2 asphyxiation followed by cervical dislocation in accordance with guidelines from the American Veterinary Medical Association (AVMA) and was approved by the Tufts IACUC.

### Bacteria

Low passage isolates of *Borrelia burgdorferi* (strain B31) were cultured in Barbour-Stoenner-Kelly II (BSK-II) complete medium at 37°C to logarithmic phase and cell density determined by using a Petroff-Hauser counting chamber.[42]

## METHOD DETAILS

### Infection of mice and preparation of tissue

Mice were inoculated subcutaneously in the center of the abdomen with $10^5$ spirochetes in 100 µl or with 100 µl BSK-II medium for uninfected controls. *B. burgdorferi* infection was confirmed by culturing of live spirochetes from the ears in BSK-II medium at time of sacrifice and visualization of spirochetes using dark-field microscopy. All mice were infected at the same time for single-cell RNA sequencing and sacrificed at indicated time points. Specifically, at two, four, six and eight weeks post-infection, 10 mice were sacrificed and ankle joints harvested. Ankle joints were processed as previously described.[12] Briefly, joint tissue was digested for 1 hour at 37°C in RPMI containing 0.2 mg/ml liberase TL (Roche) and 1 unit/ml DNase (Thermo), inverting every 15 minutes. Cells from the 10 mice used per time point were pooled and were then filtered through a 40 µm filter and washed in PBS containing 2% FBS and 1 mM $CaCl_2$. Live cells were obtained through magnetic sorting using the EasySep Dead Cell Removal (Annexin V) Kit (StemCell Technologies) per manufacturer's instructions. Following dead cell removal, cells were washed in MACS buffer (PBS containing 0.5% BSA and 2 mM EDTA) and $CD45^+$ and $CD45^-$ cells separated using CD45 MicroBeads and a MiniMACS Separator per manufacturer's instructions (Miltenyi Biotec).

### Single cell RNA library preparation and sequencing

Cells were twice washed in RPMI containing 10% FBS, counted via hemocytometer, and resuspended to a concentration of 1,000 cells/μl. Cell suspensions were loaded onto a 10x Chromium instrument with Single Cell K Chip per manufacturer's protocol with a targeted recovery of 10,000 cells per sample. Library preparation was performed with the Chromium Single Cell 5' Library and Gel Bead Kit v2 (Part Number 1000263). Library preparation was performed with the Library Construction Kit (Part Number 1000190) and samples were sequenced on an Illumina HiSeq instrument with 2x150bp sequencing. Both the $CD45^+$ and $CD45^-$ samples for each time point were sequenced immediately after library preparation.

### Single-cell RNA sequencing pre-processing

The 10x Genomics Cellranger (v.6.0.0) pipeline was used to align raw sequencing reads to the murine Mm10 reference genome (10x Genomics, v.3.0.0) to generate cell read count matrices for each sample.[49] Count matrices for each time point (both $CD45^-$ and $CD45^+$; 10 total) were read into R (v.4.1.1) using the *Seurat* package (v.4.0.5).[43] Raw read count matrices were processed with the *DropletUtils* package (v.1.14.2)[44] to exclude empty droplets using the 'emptyDrops' function, keeping only cell barcodes with an FDR < 0.01. Genes detected in fewer than 3 cells were discarded from the read matrices. Low quality cells were removed if they contained mitochondrial reads higher than 2 standard deviations above the mean and fewer than 500 unique genes detected. Counts from all samples were merged into one matrix, split by sample, and log normalized across each sample. To minimize batch effects, the top 2000 highly variable genes were selected for each sample, and then 'SelectIntegrationFeatures' was used to determine the top 2000 highly variable genes across all samples. Week 0 ($CD45^-$ and $CD45^+$) samples were used as a reference with Reciprocal Principle Component Analysis (RPCA), selecting the top 50 dimensions for integrating the datasets together (using the 'FindIntegrationAnchors' and 'IntegrateData' functions), which reduces batch-specific effects and allows for comparative scRNA-seq analysis across experimental conditions (i.e. time).[43,50] The integrated dataset was then scaled and PCA was performed, from which the top 50 dimensions were used to generate a Uniform Manifold Approximation and Projection (UMAP). Clusters were identified by constructing a Shared Nearest-Neighbor (SNN) graph using the top 50 dimensions of the PCA and 20 k-nearest neighbors with the 'FindNeighbors' function before using the Louvain algorithm for modularity optimization with 'FindClusters'.

### Clustering analysis of single cell data

Based on the parameters above, 39 unique clusters were identified. 'FindAllMarkers' was used to identify cluster-defining genes (Table S1), from which these 39 unique clusters were grouped into fibroblast-like, myeloid, lymphoid, vascular, or dividing cells based on expression of genes including *Col3a1*, *Csf1r*, *Cd79a*, *S100a9*, *Prg4*, *Cd3d*, *Cd209a*, *H2-Aa*, and *Mki67*. From these broader groups, clusters were assigned into 17 more distinct cell types using marker gene expression including the genes listed above. For macrophage, T cell, fibroblast, synoviocyte, B cell, and neutrophil clusters, sub-clustering was performed from the main population to identify heterogeneity. Each cell group to be sub-clustered was subsetted from the main population, a new set of 2000 variable features was found, the count matrices were rescaled and another PCA/UMAP was generated as above. Doublet clusters were identified from these sub-clusters based on co-expression of genes from multiple cell types (for example, co-expression of *Lyz2* and *Hbb-bs* in a macrophage/monocyte sub-cluster). Doublet clusters were removed and singlets re-clustered as above to generate the final sub-clustered population UMAP. Cluster-defining genes for each cell subset was calculated using the 'FindAllMarkers' Seurat function.

### Differential gene expression analysis

For each main cell population, we performed a pseudobulk method of differential gene expression.[51,52] From each of the 10 samples ($CD45^+$ and $CD45^-$ for the five timepoints), count matrices were summed across genes for each sub-cluster. Samples with fewer than 2 cells in a condition were dropped from analysis. $CD45^-$ and $CD45^+$ samples from the same time point were treated as replicates for pseudobulk analysis and the *DESeq2* package (v.1.38.2)[45] was used to identify differentially expressed genes. For all sub-clusters except macrophages, mitochondrial ("*mt-XX*"), ribosomal ("*RplX*" or "*RpsX*"), and poorly annotated genes ("*Gm-*") were removed from gene lists prior to differential gene analysis. In addition, for T cells and B cell sub-clusters, TCR (e.g. *Tr(a/b/g/d)(v/j)*) and immunoglobulin genes (e.g. *Ig(klh)(vmg)*), respectively, were removed prior to analysis. A likelihood ratio test (LRT) was used to compare samples over time against a reduced model taking into account cell number for each condition. To visualize gene changes over time, normalized pseudobulk counts were scaled across genes, averaged across replicates, and plotted by week. Psuedobulk data can be found in Tables S2, S4, S5, S6, S7, and S8. For clusters with too few cells to perform pseudobulk differential gene analysis, the 'FindMarkers' function was used with the Wilcoxon Rank Sum test.

### Gene set enrichment analysis

Pseudobulk analysis comparing week 0 (uninfected) to week 2 within each sub-cluster was also performed with an LRT as above. Fold changes from these comparisons were supplied for Gene Set Enrichment Analysis (GSEA) using the *fgsea* package (v.1.24.0) and tested against either the Molecular Signature Hallmark (v.7.2)[46] or GO (v.7.5.1) gene sets. As in pseudobulk analysis, certain genes were removed prior to GSEA (see above section for specific genes removed). All of the GSEA results can be found in Table S3. For M1/M2 signature analysis of MacMono sub-clusters, count matrices were summed across genes for each sub-cluster, combining weeks together. Log2 fold change was calculated on scaled pseudobulk expression for each cluster vs. every other cluster. GSEA was performed using the *fgsea* package with the previously described M1/M2 signature gene sets[11] as input.

### Cell-cell communication analysis

A publicly available library of receptor-ligand pairs was obtained from *OmniPath* (v.3.5.25, R) via the 'import_ligrecextra_interactions' function,[47] and differential expression results were then queried for these receptor-ligand pairs. Differential gene expression results were filtered to genes that were found in the library of receptor-ligand pairs that additionally had a log-fold-change > 1 (week 2 vs. week 0) and an FDR < 0.05. All unique combinations where both the receptor and ligands were differentially expressed were aggregated and can be found in Table S9. Select differentially-expressed receptor-ligand pairs where analogous ELISA data were available were visualized with the *ComplexHeatmap* package (v.2.14.0, R).[48]

### Cytokine assessment

Cytokines assessment was conducted in Helble et al.[12] and reanalyzed for this study using Prism software. Briefly, mice were infected subcutaneously with *B. burgdorferi* and ankle joints excised at specific time points. Protein was extracted and submitted to Eve Technologies for Mouse Cytokine/Chemokine 31-Plex discovery assay. Results were normalized to the total protein concentration.

### Flow cytometry analysis

Ankle joint tissue was processed into a single cell suspension as described above (see "Infection of mice and preparation of tissue"). Rather than sorting for live cells and separating $CD45^{+}/CD45^{-}$ cells, ankle joint cells were stained in MACS buffer with the following fluorochrome conjugated antibodies (all antibodies were purchased from BioLegend except where otherwise noted): CD16/32 (S17011E), CD45 (30-F11), CD3 (17A2), CD4 (GK1.5), CD44 (IM7) and a LIVE/DEAD Fixable Aqua Dead Cell Stain Kit (Invitrogen). Flow cytometry data were collected on an LSR II (BD Biosciences) and analyzed using FlowJo (Tree Star).

### Visualization

The R packages *Seurat*, *fgsea*, and *ggplot2* (v.3.4.0) were used to make all graphs pertaining to scRNA-seq. The experimental schematic was generated with BioRender. ELISA and flow cytometry data were plotted with GraphPad Prism.

## QUANTIFICATION AND STATISTICAL ANALYSIS

For cytokine assessment and flow cytometry data, differences were considered statistically significant if the *P* value was less than 0.05. Data were graphed as the means ± standard errors of the means (SEM). For all figures, * $P < 0.05$, *** $P < 0.001$, and **** $P < 0.0001$.